Article

Not peer-reviewed version

Exploring the Potential of Anastatica hierochuntica-Integrated Nanofibers as a Promising Nanoplatform for Enhanced Biofilm Disruption and Accelerated wound Healing

Eman Abdelhakeem *, Mona M. Hashem, Heba Attia, Mohamed A. Abdel Khalek, Shaimaa M. Badr-Eldin, Islam M. Adel

Posted Date: 15 October 2024

doi: 10.20944/preprints202410.1181.v1

Keywords: Anastatica hierochuntica; Biomaterials; Electrospinning; Nanofibers; Wound healing

Article

Exploring the Potential of *Anastatica hierochuntica*-Integrated Nanofibers as a Promising Nanoplatform for Enhanced Biofilm Disruption and Accelerated Wound Healing

Eman Abdelhakeem [1,*], Mona M. Hashem [2], Heba Attia [3], Mohamed A. Abdel Khalek [4], Shaimaa M. Badr-Eldin [5] and Islam M. Adel [1]

[1] Department of Pharmaceutics and Industrial Pharmacy, Faculty of Pharmacy, Cairo University, Kasr El-Aini Street, Cairo, 11562, Egypt
[2] Pharmacognosy Department, Faculty of Pharmacy, Cairo University, Kasr El-Aini Street, Cairo 11562, Egypt
[3] Microbiology and Immunology Department, Faculty of Pharmacy, Cairo University, Kasr El-Aini Street, Cairo, 11562, Egypt
[4] Institute of Nanoscience and Nanotechnology, Kafrelsheikh University, Kafrelsheikh 33516, Egypt
[5] Department of Pharmaceutics, Faculty of pharmacy, King Abdulaziz University, Jeddah, KSA
* Correspondence: eman.abdelhakeem@pharma.cu.edu.eg; Tel.: +20-1000230782

Abstract: Natural components are sparking a lot of interest in the field of drug formulation and delivery. ***Anastatica hierochuntica*** is a small plant, extremely rich in its phytochemical content including flavonoids, phenolics, and several minerals. For that, it is widely used in folk medicine in a plethora of conditions such as headache, asthma, menstrual pain, and childbirth. **The aim** of this research is to investigate its potential antimicrobial effects when loaded onto nanofiber as field leading. The extract-loaded nanofibers were prepared via electrospinning. The prepared nanofibers were rod-shaped with nanometric size as revealed by scanning electron microscopy. The loaded NFs showed increased hydrophilicity compared to the plain NFs as evidenced by reduced WCA and increased percent water uptake. Further, they exhibited adequate tensile properties compared to the plain NFs as evidenced by increased strain and stress. Based on the highest hydrophilicity (WCA **43.1±0.6º and % swelling 216.67±2.36% after 1 h**) and the best mechanical properties (strain and stress of 67.6% and 0.0486 N/mm^2, respectively), NF20 was selected for further investigations. The selected formulation (NF20) showed a bi-phasic, sustained drug release pattern (**73.40±1.31%** after 72 h). More importantly, testing the antimicrobial effects of the extract-loaded nanofibers highlighted significant reduction in MIC, MBC, and MFC values when compared with Silymarin standard against ***Acinetobacter baumannii, Pseudomonas aeruginosa, Staphylococcus aureus,*** and ***Aspergillus niger***. Finally, wound healing assay confirmed the accelerated wound closure and fibroblasts migration in case of the fabricated NF20, suggesting the potential of the bio- fabricated nanofiber as a novel promising wound dressing.

Keywords: *Anastatica hierochuntica*; biomaterials; electrospinning; nanofibers; wound healing

1. Introduction

An intact **skin** plays an indispensable role for human survival, functioning as a vital protective barrier against external pathogens and harmful substances[1]. it prevents excess water loss while preserving essential electrolytes[2]. Not less significant, the skin serves the body's sensory organ and significantly contributes to the regulation of body temperature regulation[3] For all of that and more, maintaining a healthy, intact skin is a must for human survival. Wound prevalence is a global health concern, either for acute cases or chronic conditions. Effective wound healing is critical for

 doi:10.20944/preprints202410.1181.v1

maintaining skin integrity and avoiding problems like infection and tissue damage. Timely healing promotes recovery, lowers healthcare costs, and improves patient quality of life, whereas delayed healing can pose major health hazards; Attempting to achieve rapid and efficient healing highlights the importance of advanced treatment strategies[4]. Naturally, wound healing occurs in four phases. The first phase, hemostasis, begins immediately after injury, increasing blood flow to remove pathogens and initiating clot formation to prevent excessive bleeding[5]. The second phase, inflammation, involves neutrophils and macrophages clearing pathogens, while cytokines and growth factors promote cell proliferation[6]. In complicated wounds, anti-inflammatory agents may be prescribed to prevent prolonged inflammation[6]. The third phase, tissue proliferation, sees the formation of a new extracellular matrix (ECM) and collagen deposits, which support tissue structure and angiogenesis[7]. Lastly, during remodeling, the granulation tissue matures, and blood vessels restore normal function as inflammatory cells die[8].

In order to stop bleeding, absorb excess exudates, and promote wound healing, a wound dressing is applied[9]. A wound dressing can be either simple traditional one to protect the wound solely, or an advanced one that actively participates in the wound healing and tissue regeneration process. Clearly, an advanced dressing is the optimal choice, albeit more expensive so it is generally reserved for complicated wounds[10]. While simple dressings are made of gauze or cotton, advanced dressings are usually fabricated from biomaterials. Ideally, a wound dressing should be biocompatible, biodegradable, nontoxic, nonirritant, of tailorable mechanical properties, and with good water and gas exchange properties[8]. Several agents can be added to the dressing to hasten the healing process and prevent the formation of a permanent scar; such agents include anti-inflammatory, antimicrobial, antifungal and growth promoters.

Among the favorable candidates for wound dressings are electrospun nanofibrous sheets. **Nanofibers (NFs)** have emerged as promising one-dimensional fiber-shaped nanomaterial with wide range of research and industrial applications due to their distinct features[11]. They are considered ideal wound dressings as they closely resemble the structure of the natural ECM of the skin [3,12]. They provide large surface area which facilitates higher drug loading capacities[13]. Additionally, NFs have high porosity which enables high rates of gaseous and water exchange[14]. A plethora of biomaterials can be used in NFs fabrication which ensures fine tuning of properties such as degradability and mechanical properties. On top of that, the process of electrospinning is rather a simple and easily scalable technique[15]. Thermoplastic polyurethane (TPU) is a synthetic biomaterial with good biocompatibility, minimal toxicity, and excellent mechanical behavior[16,17]. Such properties highlight the benefits of suggesting TPU as suitable biomaterial for NFs fabrication.

Anastatica hierochuntica **(***A. hierochuntica*) is a well-known medicinal plant with various medicinal uses[18]. For starters, it is commonly used to ease child delivery, alleviate menstrual cramps and hemorrhages[19]. Not only that, but *A. hierochuntica* can be used in diabetes, asthma, headache, fever, GIT disturbances, epilepsy, and heart diseases[20–22]. Such numerous uses are attributed to its rich content of minerals such as Magnesium (Mg), Calcium (Ca), Manganese (Mn), Iron (Fe), Copper (Cu), and Zinc (Zn) as well as various flavonoids, phenolic compounds[23,24]. Owing to the large combination of ingredients, *A. hierochuntica* exerts antioxidant, anti-inflammatory, antimicrobial, anti-hepatotoxic, anti-cancer, and even growth promotion effects[21,23,25]. Previous studies indicated that extracts derived from *A. hierochuntica* exhibit significant antibacterial activity against a variety of pathogenic bacteria, including *Staphylococcus aureus*, and *Pseudomonas aeruginosa*[26]. The antimicrobial mechanisms were primarily attributed to its rich phytochemical composition, which includes flavonoids, tannins, and phenolic compounds. These bioactive molecules disrupt bacterial cell membranes, leading to increased permeability and, ultimately, cell death. Furthermore, *A. hierochuntica* extracts demonstrated remarkable antifungal activity against pathogens like *Candida albicans* and *Aspergillus niger* effectively inhibiting their growth[27]. The antifungal action is believed to result from the interference with fungal cell wall synthesis and metabolic processes. By significantly reducing the viability of both bacteria and fungi, *A. Hierochuntica* extract, not only helps to prevent infections, but also enhances the healing process in

 doi:10.20944/preprints202410.1181.v1

wounds, thereby highlighting its potential as a natural antimicrobial agent in wound dressing formulations.

While previous studies have explored various natural materials for wound healing, to the best of our knowledge, no previous study has assessed the antimicrobial properties of *Anastatica* extracts in a nanofiber format. By leveraging the unique characteristics of *Anastatica*, including its bioactive compounds, in conjunction to the benefits of nanofibers, this study aimed to demonstrate not only the effectiveness of the developed nanofibers in inhibiting microbial growth but also its potential to enhance the wound healing process. The developed formulations were characterized for morphology, water contact angle, mechanical properties, as well as swelling behavior. Surface morphology of the fabricated NFs was scanned using SEM. The selected NF formulation was then tested for functional groups interaction via FT-IR scanning as well as *in-vitro* release behavior. The antimicrobial activity of the selected formulation was assessed against *Acinetobacter baumannii, Pseudomonas aeruginosa, Staphylococcus aureus*, and *Aspergillus niger*. Finally, Scratch assay was carried using human fibroblasts cell line to assess wound closure and cell migration.

2. Materials and Methods

2.1. Materials

Plant material

Anastatica hierochuntica L. (Kaff Maryam) was obtained from a local herb supplier; Harraz Market for Medicinal Herbs, Cairo, Egypt. The sample was authenticated by Eng. Threase Labib, consultant in Orman Garden and National Gene Bank, Ministry of Agriculture. A voucher specimen (No. 10-7-2023-F) was kept at the Herbarium of Pharmacognosy Department, Faculty of Pharmacy, Cairo University.

Chemicals

Human skin fibroblasts (HSF; CCD-1112SK) cell line was procured from American Type Culture Collection (ATCC), Rockville, MD, USA. Thermoplastic Polyurethane (TPU), and Chloroform were purchased from LANXESS AG, Germany. Dimethylformamide (DMF) was purchased from Thermo Fischer, Germany. All other solvents were of analytical grade.

2.2. Quantification of Silymarin Components in the Total Methanolic Extract of Anastatica hierochuntica

2.2.1. Stock Preparation of the Total Methanolic Extract and Silymarin Components

A stock solution of pure total methanolic extract was prepared using methanol (1mg/mL). The same procedure was followed for Silymarin standard, to prepare a stock solution of concentration of 100 µg/mL. Eight calibration standards of Silymarin were prepared in separate volumetric flasks (1, 2.5, 5, 10, 20, 40, 80, and 100 µg/mL) and used later to construct the calibration curves. One mL of each was transferred to HPLC opaque vials before injection.

2.2.2. Instrument and Chromatographic Parameters

Thermo Fisher UPLC-DAD Ultimate 3000 (USA) was employed using a Hypersil Gold column with dimensions (250 × 4.6) particle size 5 µm. A mixture of (0.1% orthophosphoric acid water) as (A) and (100 % acetonitrile) as (B) was applied in increasing gradients as follows: 0–3 min (10% B), 3-40 min (15% B), 40–60 min (35% B), and 60-62 min (10% B). A stable flow rate of 0.5 mL/min was used over the sixty-two-minute run. The same gradient condition was used to determine Silymarin calibration standard. Standard silymarin was eluted in four consecutive peaks at 24.10 Min, 33.00 min, 44.00 min, and 45.80 min corresponding to silychristin, silydianin, silibinin (silybin), and isosilibinin (isosilybin), respectively. This elution sequence of the peaks was validated over the precise determination of the four obtained Silymarin peaks with previously published results on identical Silymarin standard utilizing the same mixture of acidic water and acetonitrile increasing gradient[28]. Thereupon, calibration curves were constructed for each of the four peaks out of the standard Silymarin. Statistical t-test within the Silymarin standard was computed. The obtained results showed no significant difference between the means of the groups that certify a valid

 doi:10.20944/preprints202410.1181.v1

reproducible similarity. UV detection was carried out at 289 nm and a column temperature of 25ºC prompted optimal peak intensity[28]. Five different stock batches of plant extract were prepared according to the mentioned conditions before injection in triplicates. Identical fingerprint chromatograms were obtained achieving the same detection sequence. Correlating the standard chromatogram of Silymarin with peaks resulted in plant extract chromatograms, silychristin, silydianin, silibinin, and isosilibinin peaks were conclusively identified as the essential chemical markers in extract matrix. The calibration curves were then used to determine the concentration of silychristin, silydianin, silibinin, and isosilibinin in 1mg/mL of the extract.

2.3. Fabrication of Anastatica hierochuntica Extract-Loaded TPU-Based Nanofibers

2.3.1. Preparation of the Spinning Solution

Initially, TPU solution was prepared by dissolving TPU pellets in a mixture of DMF/Chloroform (3: 1 %v/v) under magnetic stirring at 600 rpm (Stuart, SB162, UK) till a clear solution was obtained. Following, the lyophilized extract solution was dissolved in the prepared TPU solution under magnetic stirring at 600 rpm for 5 h. The process variables were set, where concentrations of TPU and the extract were varied and tested.

2.3.2. The Electrospinning Process

Immediately after the preparation of the spinning solution, NFs were fabricated using an electrospinning device (spinneret). The prepared solution was first loaded into a 10 mL syringe (I.D. of 14.5 mm) attached to a pump. The collector plate, at the other end, was fixed at a distance of 10 cm, and covered with aluminum foil. After the initial preparation was carried out, the flow rate was adjusted to 1 mL/ h and the syringe pump (Era Pump Systems NE-1000) was started. Immediately on the appearance of the first droplet on the tip of the syringe, the power supply unit (Spellman High Voltage CZE1000R Series) was operated at 15 kV to create an electrical voltage difference between the syringe tip and the collector plate. Elongation of the polymer solution took place due to the increase in polymer surface charge, exceeding its surface tension, and on the volatilization of the solvent, that led to the deposition of the NFs on the collector plate[30]. The deposited NFs were allowed to air-dry for 24 h to ensure the complete removal of solvent residuals prior to further testing.

2.4. Characterization of the Fabricated Nanofibers

2.4.1. Evaluation of Nanofibers Morphology and Surface Roughness

Surface morphological characteristics were evaluated using scanning electron microscope (SEM; Tescan Vega 3 SBU, Czech Republic) operated at 30 kV. Briefly, precise cuts from the NFs were fixed using a carbon tape onto stubs then sputter coated (Quorum techniques Ltd., sputter coater, Q150t, England) with gold for few minutes. The prepared specimens were then visualized, and images were recorded at a magnification power of 30 kV. Histograms representing surface roughness were drawn using OriginLab Analysis & Graphing Software.

2.4.2. Static Water Contact Angle (WCA)

Measurement of WCA was carried to evaluate the wetting behavior of the fabricated NFs (NFP, NF10, and NF20) using the sessile drop method[30]. Briefly, a 2 cm × 2 cm sample was precisely cut from the prepared NFs and carefully fixed on a glass strap. Following, a drop of water (10 µL) was dropped using a microsyringe on the fixed sample and images were captured using the attached camera and WCA was measured using an OCA 15EC Contact angle Goniometer (DataPhysics Instruments GmbH)

2.4.3. Mechanical Properties

The tensile strength of TPU-based NFs (NFP, NF10, and NF20) was studied to evaluate their suitability for wound dressing application. The selected formulations were cut into rectangular

 doi:10.20944/preprints202410.1181.v1

samples having dimensions of 35 mm × 25 mm × 1 mm (L×W×H). Following, samples were placed between the wedges of a Universal Testing Machine (Shimadzu, Autograph AG-X plus, Japan) and the crosshead speed was set to 2 mm/min. Data obtained was represented in the form of stress-strain curve.

2.4.4. Percentage Water Uptake (%W_u)

The swelling behavior of the fabricated NFs (NFP, NF10, and NF20) was studied by carrying water uptake assay. Initially, precise cuts of the fabricated NFs (2 cm × 2 cm) were oven-dried at 40℃ to ensure complete water removal and the dry weights were recorded (W_0). Secondly, the dry NFs were immersed in petri dishes filled with equal volumes of distilled water (20 mL) and placed in an incubator at 37±0.2℃. After 1 h, the soaked samples were taken out of the petri dishes, plotted against filter papers and re-weighed (W_t). %W_u was calculated according to the following equation[31].

$$\%W_u = \frac{W_t - W_0}{W_0} \times 100$$

2.4.5. Fourier-Transform Infrared Spectroscopy (FT-IR)

Scanning of FT-IR spectra for NFP and the selected NFs (NF20) was run to detect possible interactions between their functional groups (if any). Accurately weighed samples (3 mg) were mixed with potassium bromide and casted against the walls of a small disc. IR spectra were recorded for extract-loaded NFs as well as plain NFs using FT-IR spectrophotometry (Model, 8400 s Shimadzu, Kyoto, Japan) run over a range of 4000 – 400 cm^{-1}.

2.4.6. Inspection of In-Vitro Release Behavior

Assessment of the release behavior from the selected NFs (NF20) was carried via the dialysis bag method[32,33]. Briefly, precisely cut NF mat (1 cm × 1 cm; equivalent to 5 mg of the dry extract) was placed in a dialysis cellulose bag, presoaked in distilled water overnight and carefully locked from one end. A 1 mL of phosphate buffer saline (PBS; pH 7.4) was added to the NF mat and immediately, the bag was tightly locked from the other end. Following, the assembly was placed in a 50 mL glass bottle prefilled with 25 mL of PBS as the release medium to ensure sink conditions were met. The glass bottle was transferred to a thermostatically controlled water bath (Unimax, IKA, Germany) and running parameters were set to 37±0.2℃ and 50 rpm. At select intervals, 3 mL samples were withdrawn and analyzed for the extract content using a UV Spectrophotometer (model UV-1601 PC; Shimadzu, Kyoto, Japan) at λ_{max} 292 nm. Data obtained was represented graphically as % drug released vs time. The preceding procedure was repeated on the alcoholic extract solution for comparative purpose.

2.5. Microbiological Assay

2.5.1. Selection of Bacterial and Fungal Strains

In this study, *Acinetobacter baumannii* (ATCC 19606) and *Pseudomonas aeruginosa* (PAO1 strain; ATCC 87110) were selected as the tested Gram-negative bacterial strains, while *Staphylococcus aureus* (ATCC 25923) was selected as the tested Gram-positive bacterial strain, and *Aspergillus niger* (ATCC 32656) as the tested fungal strain. Brain heart Agar (BHA) and double strength Muller-Hinton Broth (Oxoid, Hampshire, UK) were used as the growth media for the tested bacterial strains. All plates and test tubes were incubated for 18-24 h at 37ºC. Sabouraud Dextrose Agar (SDA) and Sabouraud Dextrose Broth (SDB) (Oxoid, Hampshire, UK) were used as the growth media for the fungal strain. All plates and test tubes were incubated for 48–96 h at 28±2ºC.

 doi:10.20944/preprints202410.1181.v1

2.5.2. Determination of Minimum Inhibitory Concentration (MIC)

Minimum inhibitory concentration was determined by Resazurin-based 96-well plate microdilution technique in accordance with the Clinical and Laboratory Standards Institute guidelines[34]. All tested extracts and preparations were dissolved in dimethyl-sulfoxide (DMSO). Two-fold serial dilutions of the *A. hierochuntica* extract, the selected NFs (NF20), and Silymarin standard, in concentration ranges (100–0.195 mg/mL), (30-0.058 mg/mL), and (25–0.0488 mg/mL) respectively, were prepared in 100 µL double strength MHB- for all tested bacterial strains-, or 100 µL double strength SDB- for the tested fungal strain. The serially diluted preparations were dispensed into U-shaped bottom, sterile 96-well plates. Then, 20 µL of the bacterial or fungal suspension (inoculum size of 10^5–10^6 CFU/mL) was added to each well. After that, the microtiter plates were incubated at 37ºC for 24 h for the bacterial strains, and at 28±2 ºC for 48–96 h for the fungal strain. Following, turbidity in each well was recorded, and the absorbance was measured at a wavelength of 600 nm using a 96-well plate reader. Moreover, 30 µL of 0.01% Resazurin solution was added to each well then, plates were incubated again for 2-4 h at 37ºC for the observation of color change. After the incubation, wells with no color change (blue resazurin color persisted) were scored as negative microbial growth, and wells with a color change to pink was scored positive microbial growth. The MIC was determined as the lowest concentration showing no observable growth and unchanged blue color. Negative control (control for the sterility of the media), positive control (microbial growth control), blank control (NFP), vehicle control (DMSO), and color control (to account for the color absorbance) were performed. Tests were performed in triplicates (biological and technical replica). Differences between MIC values were analyzed for statistical significance in version 4.1.2 of R by the Kruskal–Wallis test, followed by post-hoc pairwise Wilcoxon testing. ns = non-significant (p value > 0.05); ** = p value < 0.005; * = p value < 0.05.

2.5.3. Determination of Minimum Bactericidal Concentration (MBC) and Minimum Fungicidal Concentration (MFC)

The determination of MBC and MFC was performed by broth microdilution method according to the guidelines of the Clinical and Laboratory Standards Institute. Briefly, for MBC determination, Two-fold serially diluted preparations with 20 µL bacterial inoculum suspension (inoculum size of 10^5–10^6 CFU/mL) were incubated in 96-well plates at 37ºC for 24 h. Then, on the surface of Muller-Hinton Agar media plates, 10 µL of the mixture of bacterial inocula and the two-fold serially diluted preparations were spotted till the concentration of its MIC. Similarly, for MFC determination, the same method was applied by using Sabouraud Dextrose Agar (SDA) plates which were incubated at 28±2ºC for 48-96 h.

The MBC/MFC was expressed as the lowest concentration showing no visible growth. Biological and technical triplicates of the experiment were conducted. The statistics were performed in version 4.1.2 of R by the Kruskal–Wallis test, followed by post-hoc pairwise Wilcoxon testing. ns = non-significant (p value > 0.05); ** = p value < 0.005.

2.5.4. Investigating the Biofilm Inhibitory Effect via Crystal Violet Technique

The changes in the tested bacterial standard strain biofilm formation in the presence of *A. hierochuntica* extract, the selected NFs (NF20), and Silymarin standard were determined as described before[35,36]. Briefly, an equal volume of bacterial suspension (10^8 CFU/mL in MHB) and the tested compound were loaded in sterile 96-well non pyrogenic polystyrene culture flat-bottom plates (total volume is 100 µL/well), so the final drug dilutions in the wells represent $^1/_{16}$, $^1/_8$, ¼, and ½, 1, 2, and 4X where X is the calculated MIC. The plates were then statically incubated at 37ºC for 24 h. Negative, positive and color controls were performed. After incubation, the optical density ($O.D_{600}$) of the bacterial culture was measured by an automated spectrophotometric plate reader (Biotek, Synergy 2, USA). The formed biofilms were quantified as follows; the supernatants were gently removed, and the wells were washed twice with sterile saline and then the plates were left to dry thoroughly. The dried formed biofilm was stained with crystal violet (125 µL, 0.5% w/v) for 30 min at room

 doi:10.20944/preprints202410.1181.v1

temperature. After the 30 min incubation, the plates were carefully washed three times with sterile distilled water and dried thoroughly. The crystal violet in the stained biofilm was solubilized by addition of 150 µL 95% w/v ethanol and incubation for 15 min with shaking (110 rpm). At the end of the experiment, the OD_{570} of the solubilized crystal violet solution was measured by the automated spectrophotometric plate reader (Synergy2) and divided by OD_{600} of the planktonic cultures for normalization. The experiment was done in technical triplicates and repeated three independent times. Results were presented as biofilm inhibition percentage and the biofilm inhibition percentage was calculated using the following equation:

$$\text{Biofilm inhibition } \% = \frac{\text{OD Control} - \text{OD Test}}{\text{OD Control}} \times 100$$

The statistics were performed in version 4.1.2 of R and visualized in Rstudio by the student's t-test[37].

2.6. Cell-line Studies

2.6.1. Cell-Line Preparation

HSF cell line (CCD-1112SK) was cultured in Dulbecco's modified eagle's medium (DMEM) supplied with 5% fetal bovine serum (FBS). Cells were maintained in humidified environment at 37±0.2℃, in the presence of 5% CO_2, and with regularly sub-cultured until usage.

2.6.2. Wound Healing Assay (Scratch Assay)

To perform the assay, the following protocol was followed[38,39]. Briefly, HSF cells were seeded at a concentration of 5×10^5 cells/well in a 6-well plate and incubated overnight under the same conditions of cultivation to allow complete cellular spreading. The next day, culture medium was removed, adherent sheets of cells in every well were gently scratched using a 10 µL pipette tip sterilized with ethanol and washed with PBS. Following, 3 mL of low-treatment medium (DMEM supplied with 1% FBS) were added to each well, followed by addition of the drug at doses corresponding to each compound's IC_{30}. In case of the selected NFs (NF20), precise micro-cuts containing the extract equivalent to IC_{30} were placed. As for NFP, micro-cuts of similar areas were used. No intervention was done in case of control group. Finally, images representing distances of cellular migration into the wound space were captured at different intervals (0, 24, 48, and 72 post-treatment) using an inverted microscope equipped with an optical camera (ZEISS ZEN microscope, software blue edition). Parameters were calculated to detect differences between the groups on wound healing which included wound closure % and % cell migration, according to the following equations:

For wound closure %[40];

$$\% \, \mathbf{WC} = \frac{(\mathbf{A_0} - \mathbf{A_t})}{\mathbf{A_0}} \times \mathbf{100}$$

Where % WC is wound closure percentage, A_0 is the initial wound area (at time zero), while A_t is the wound area at any given time.

2.7. Statistical Analysis

Data analysis was carried using SPSS® software (SPSS Inc., 26.00 IBM Corporation, NY, USA). One-way analysis of variance (ANOVA) was the test of choice to detect significance (P value < 0.05), coupled with least significance difference (LSD) to detect difference between groups, unless stated otherwise. All trials were carried in triplicates (n=3) and data was represented as mean±S.D.

 doi:10.20944/preprints202410.1181.v1

3. Results and Discussion

3.1. Silymarin Components Quantification

Upon quantification of different Silymarin components *viz.* silychristin, silydianin, isosilibinin and silibinin in the total methanolic extract of *A. heriochuntica*, the results revealed the enrichment of the methanolic extract with mainly silychristin, followed by isosilbinin, then silydianin, and finally silibinin, recording values 321.73, 26.16, 12.66, and 0.43 µg per 1 mg of the total methanolic extract, respectively.

3.2. Characterization of the Fabricated Nanofibers

3.2.1. Evaluation of Nanofibers Morphology and Surface Roughness

It is critical to study surface morphology and determine NF diameter as a first step, before carrying further characterization. Surface morphology of the fabricated NFs was scanned using SEM and the results are depicted in Figure $1A_1$, $1B_1$ and $1C_1$ for NFP, NF10, and NF20, respectively. As apparent from the SEM images, the fabricated NFs are rod-shaped with overall smooth surfaces albeit, images of the extract loaded NFs demonstrate very minute ridges. This indicates the entrapment of the extract within the NF matrix while the minute ridges can be credited to the possibility of small portion being adsorbed on the surface. That coincides well with the diameter measurement of NFs where the average values of NFs diameters increased with the incorporation of the extract (150-200 nm, Figure $1B_2$) as compared to the plain formulation (180-120 nm, Figure $1A_2$). Increasing extract concentration marked another hike in NFs diameter (220-240 nm in Figure $1C_2$ vs 150-200 nm in Figure $1B_2$). Additionally, the histograms for surface roughness in Figure $1A_3$, $1B_3$ and $1C_3$ are in good agreement with SEM findings. Visualizing the histograms, a marked inflation in Figure $1C_3$ can be noticed as compared to $1B_3$ and $1A_3$, confirming the effect of added extract on NFs diameter. On the other hand, there is a visible increase in the density of surface ridges upon increasing the extract concentration which suggests increased extract residue on the surface. Increased surface roughness indicates increased NFs hydrophilicity owing to the numerous hydrophilic phenolic groups within the extract backbone[41,42].

 doi:10.20944/preprints202410.1181.v1

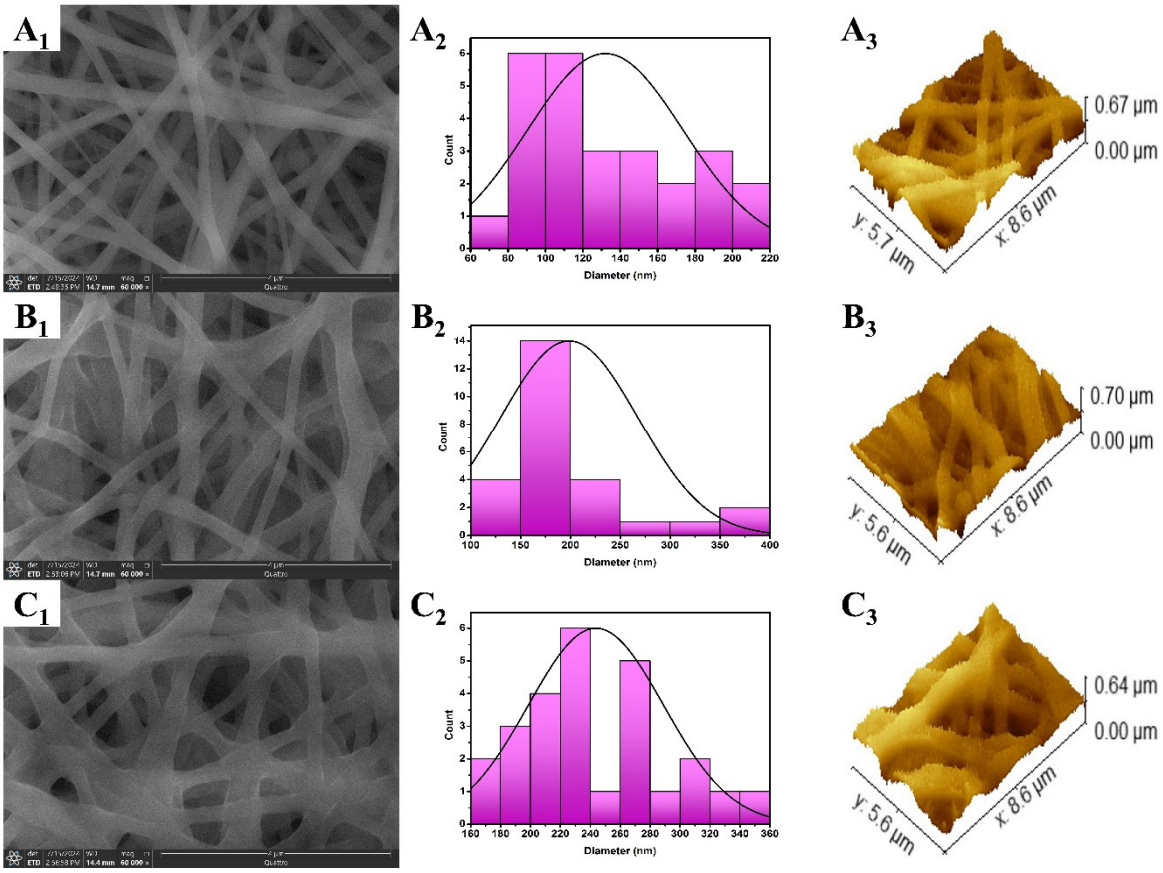

Figure 1. SEM images of the fabricated NFs showcasing the rod-shaped NFs with an overall smooth surface. Minute ridges are seen in case of the extract-loaded NFs. The images also illustrate the difference in diameter of the fabricated compared plain (A), 10% extract loaded NFs (B), and 20% extract loaded NFs (C).

3.2.2. Static Water Contact Angle (WCA)

Measurement of WCA is critical to determine surface hydrophilicity of the fabricated NFs where a reduced WCA reflects an enhanced hydrophilicity. Generally, the efficiency of a wound dressing is largely dependent on its surface hydrophilicity. From one perspective, increased surface hydrophilicity is favorable in early stages of wound healing where rapid drainage of wound exudates favors accelerated wound healing[43,44]. From a different perspective, excessive rise in surface hydrophilicity hinders the attachment of hydrophobic bacteria (such as S. aureus) and hence, retard the anticipated antimicrobial properties of the wound dressing[41,42]. Figure 2. demonstrates the effect of extract loading within the matrices of the fabricated NFs. As expected, NFP demonstrated large WCA of 86.7±0.75º (Figure 2A) due to the hydrophobicity of TPU. Incorporation of the extract resulted in significant reduction in WCA to 65.7±0.4º (Figure 2B) and 43.1±0.6º (Figure 2C) for NF10 and NF20, respectively. The increased hydrophilicity associated with increasing the extract concentration can be explained based on the abundance of the water-soluble phenolic groups in the extract[45]. Overall, a WCA in the range of 40-70º is considered ideal to promote cellular adhesion and enhance wound healing[41].

 doi:10.20944/preprints202410.1181.v1

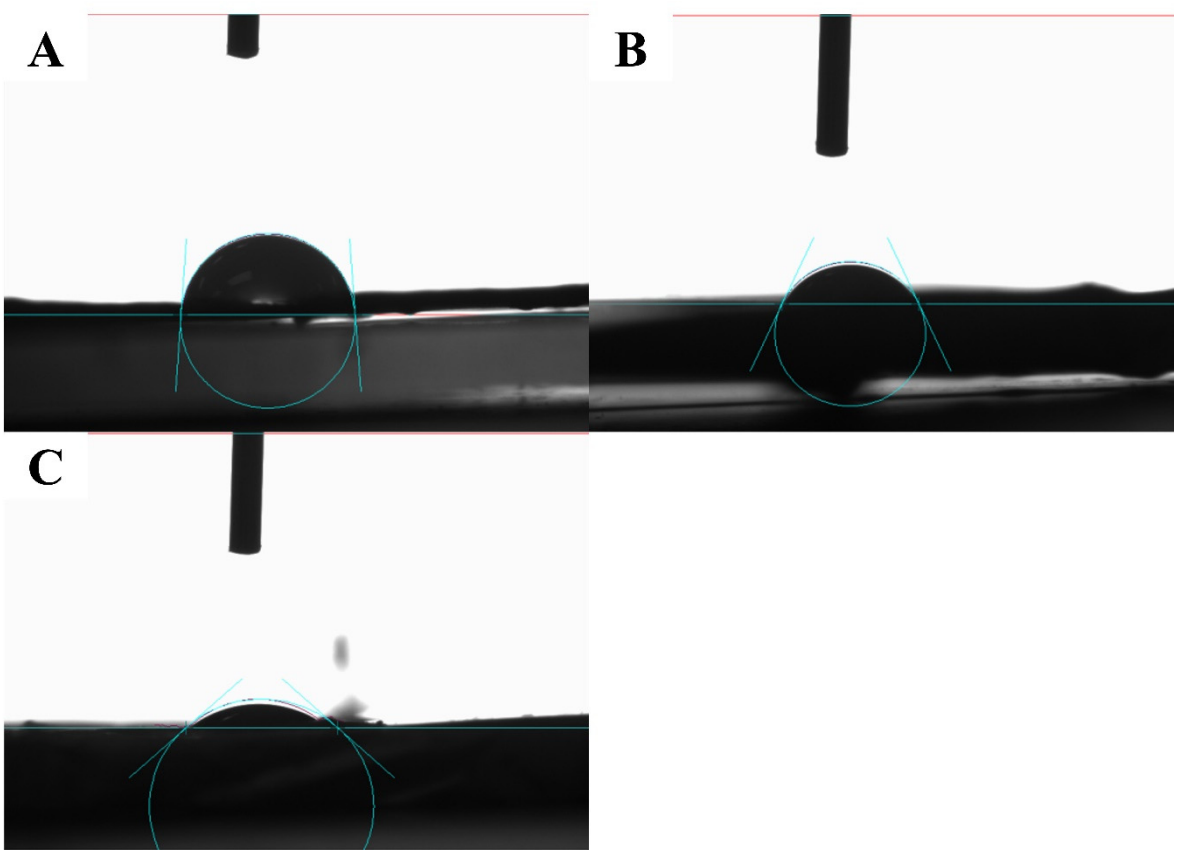

Figure 2. WCA measurements of NFP (A), NF10 (B), and NF20 (C). The images highlight the reduction in WCA with the inclusion and/or increasing the amount of the loaded extract.

3.2.3. Mechanical Properties

The stress-strain curves of the tested samples are depicted in Figure 3. while the data is highlighted in Table 1. Based on the curves and the data obtained from the software, it is evident that the extract-loaded NFs demonstrate significantly larger deformability and elasticity, as indicated by the much larger values of strain (15.1%, 45.6%, and 67.6% for NFP; Figure 3A, NF10; Figure 3B, and NF20; Figure 3C, respectively). Not only that, but the increase in stress values of the extract-loaded NFs (0.0396 N/mm^2 and 0.0486 N/mm^2 for NF10 and NF20, respectively) compared to the plain ones (0.012 N/mm^2) suggests their improved capabilities of withstanding the applied force. The abundance of hydroxyl functional groups within the structure of *A. hierochuntica* could be the key point for explaining this finding; the hydroxyl groups could be entrapped within TPU backbone, and they are capable of forming several hydrogen bonding with TPU. Such interaction is responsible for the increased rigidity of the polymer network in the extract-loaded NFs. Moreover, increasing the concentration of the extract implies further extract-polymer interaction and even more rigidity, being added to the polymer skeleton. Young's modulus was calculated and found to be 86.9 for NF10 and 71.9 kPa for NF20. Such values lie in the normal range of human skin elasticity values (5 kPa-140 MPa)[46]. To conclude, the addition of *A. hierochuntica* has brought a meaningful improvement to the overall tensile properties of the highly elastic TPU.

 doi:10.20944/preprints202410.1181.v1

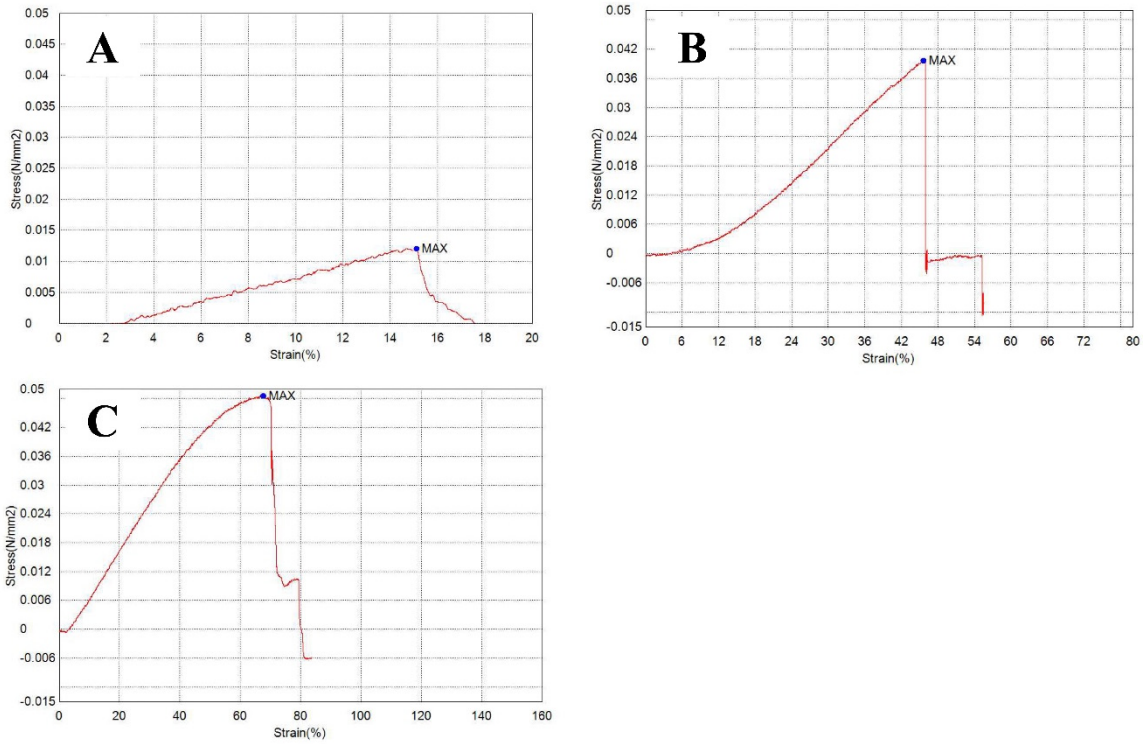

Figure 3. Stress-strain curves of the fabricated plain NFP (A), 10% extract loaded (B), and 20% extract loaded NFs (C). The curves reveal the effect of the extract loading onto increased elasticity and ability to withstand the applied force.

Table 1. Characterization of the Fabricated NFs.

Formulation	Characterization			
	Tensile Strength			Maximum $\%W_u$
	Strain (%)	Stress (N/mm^2)	Young's modulus (kPa)	
NFP	15.1014	0.01204	79.7277	66.67±2.36
NF10	45.6111	0.03964	86.9087	122.5±3.54
NF20	67.5833	0.04859	71.8965	216.67±2.36

Abbreviations: NFs, Nanofibers; NFP, Plain Nanofibers; NF10, 10% extract-loaded nanofibers; NF20, 20% extract-loaded nanofibers; $\%W_u$, percentage water uptake.

3.2.4. Percentage Water Uptake ($\%W_u$)

Carrying water uptake test is of utmost significance when it comes to wound dressings. Not only does water uptake causes dressing swelling which could potentially affect drug release[47], but also it prevents the excessive loss of tissue exudates with the accompanying load of nutrients and O_2[48]. The preservation of nutrients and O_2 in-situ enhances the rate of wound healing and lessens the chances of fibrosis and permanent scars. Data for water uptake is represented in Table 1. It can be seen that the incorporation of *A. hierochuntica* extract produced a 1.8- and a 3.2-fold rise in $\%W_u$ for

 doi:10.20944/preprints202410.1181.v1

NF10 and NF20, respectively, when compared to NFP (%W_u for NFP, NF10, and NF20 are $66.67 \pm 2.36\%$, $122.5 \pm 3.54\%$, and 216.67 ± 2.36, respectively). That, again, was attributed to the abundance of the hydrophilic hydroxyl groups in *A. hierochuntica* backbone that are capable of forming multiple hydrogen bonds, facilitating interaction with and uptake of water molecules. Similar findings were reported by Suryamathi et al.[49] upon incorporating the hydrophilic *Tridax Procumbens* into polycaprolactone-based NFs. In addition, doubling the extract amount in NF20 have brought a 1.77-fold rise in %W_u against NF10. Such rise was pertaining to the increased number of available hydroxyl group in the polymer matrix. The aforementioned results suggest the potential of the developed extract-loaded NFs as wound dressing.

Based on the findings from the previous tests, NF20 was selected as the nanofiber formulation of choice for further testing. The choice was based on its enhanced surface hydrophilicity as revealed by surface roughness histograms and WCA measurements. Enhanced surface hydrophilicity was confirmed by the improved water uptake capacity as compared to NF10.

3.2.5. Fourier-Transform Infrared Spectroscopy (FT-IR)

Figure 4 highlights the FT-IR spectra for NFP and NF20. The spectrum of NFP (Figure 4A) shows a broad peak at 3500-3300 cm^{-1} corresponding to the stretching NH group. The peaks at 2920 and 2859 cm^{-1} are due to the symmetric and asymmetric CH_2 group. Following, the peaks at 1744 and 1705 cm^{-1} represent the free and hydrogen-bonded carbonyl groups, respectively. finally, the sharp peak at 1531 cm^{-1} is due to the bending NH group while that at 1258 cm^{-1} is related to the stretching CN vibrations. Overall, our findings correlate well with those in the literature[50,51]. Looking at the spectrum of NF20 (Figure 4B) reveals the same peaks as those of NFP, albeit with slight shift in wavelengths and minor reduction in intensity. This observation suggests the hydrogen bond interaction between the hydrophilic functional group of the extract with TPU backbone functional groups; further, it supports the mechanical properties assessment results and the rigid characteristic of the loaded NFs.

 doi:10.20944/preprints202410.1181.v1

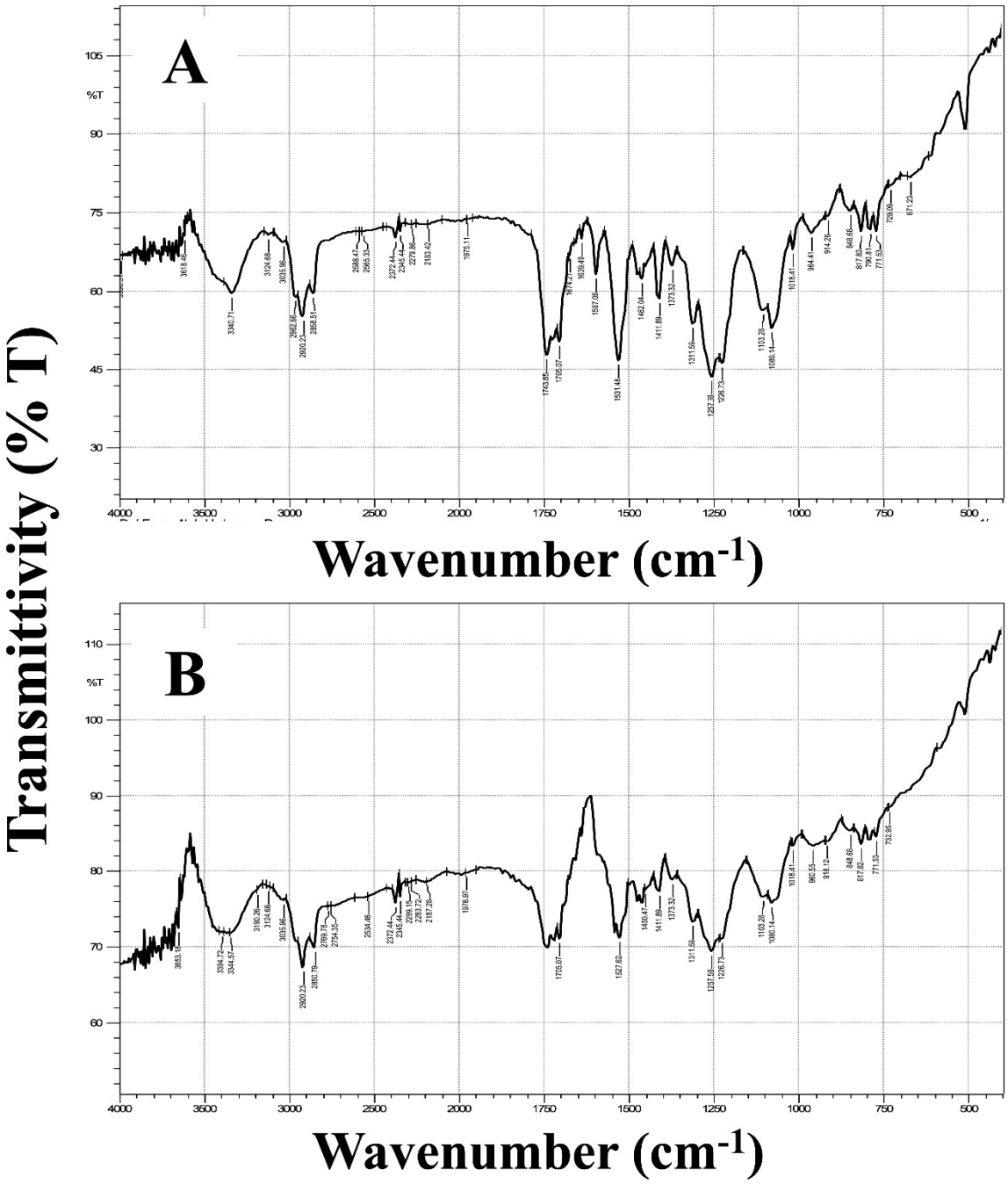

Figure 4. FT-IR spectra of the fabricated compared plain (A) and the selected NFs (B) confirming the hydrogen bond interaction between hydrophilic groups of the extract with the functiona groups of TPU polymer.

3.2.6. Inspection of In-Vitro Release Behavior

Inspecting the % drug release vs time curve in Figure 5, a biphasic release pattern can be observed for the extract-loaded NFs. An initial rapid drug release (Q_{8h} = 31.54±0.44%) was brought by the release of extract adsorbed onto or entrapped within the surface layers of the fabricated NFs. A sustainment of release was noticed on a 3-day observational period (Q_{72h} = 73.40±1.31%) that was attributed to slow drug diffusion through the polymer matrix after the initial burst duration. On comparison, drug release from the alcoholic extract was at constant pace during the same testing period. It was evident that the incorporation of *A. hierochuntica* extract within the TPU matrix has significantly delayed drug release ($p < 0.05$), as evident by comparison to its alcoholic solution. That

 doi:10.20944/preprints202410.1181.v1

holds true for Q_{8h} values (31.54±0.44% for NF20 vs 58.30±0.45% for alcoholic solution), for Q_{24} values (44.77±0.87% for NF20 vs 91.73±1.90% for alcoholic solution), as well as for Q_{48h} values (58.72±1.16% for NFs vs 96.09±3.36% for alcoholic solution). On top of that, at 72 h, drug release was nearly complete from the alcoholic solution (99.87 ± 3.36%) while it was still incomplete for NF20 (73.40±1.31%). Conclusively, extract incorporation in NFs matrix has significantly reduced release rates as compared to its alcoholic solution counterpart, implying possibility of reduced dosage frequencies and enhanced patient compliance.

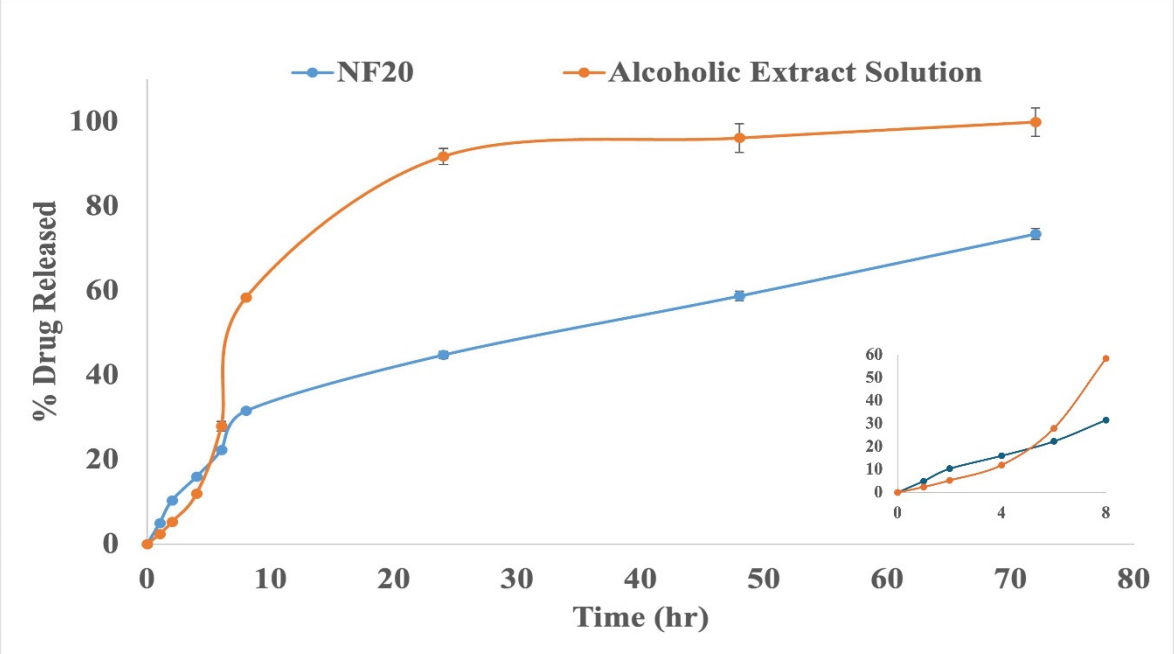

Figure 5. In-vitro release profile of *A. hierochuntica* extract from the selected NFs (NF20) as well as its pure alcoholic solution, represented as % drug release against time.

3.3. Microbiological Assay

3.3.1. Determination of Minimum Inhibitory Concentration (MIC)

MIC was determined by Resazurin-based 96-well plate microbroth dilution technique to evaluate the potential enhancement of antimicrobial activity of the selected nanofiber formulation (NF20) compared to the alcoholic extract solution, and to investigate the difference in antimicrobial efficacy between the extract and one of its main active components, Silymarin. For *Acinetobacter baumannii* standard strain, the MICs of the NF20 and Silymarin (1.875 mg/mL and 4.166 mg/mL, respectively) were significantly lower than that of the extract (16.6 mg/mL) (Figure 6A). Similarly, the MICs of NF20 and Silymarin (1.89 mg/mL and 5.208 mg/mL, respectively) were significantly lower than that of the extract (8.75 mg/mL) when tested against *Pseudomonas aeruginosa* PAO1 (Figure 6B). For *Aspergillus niger* standard strain, the MICs of NF20 and Silymarin (2.5 mg/mL and 5.2 mg/mL, respectively) were likewise significantly lower than that of the extract (9.6 mg/mL) (Figure 6D). However, only the MIC of NF20 (3.125 mg/mL) was significantly lower than that of the extract (16.6 mg/mL); there was no significant difference between the MIC of NF20 and that of Silymarin (12.5 mg/mL) (Figure 6C).

 doi:10.20944/preprints202410.1181.v1

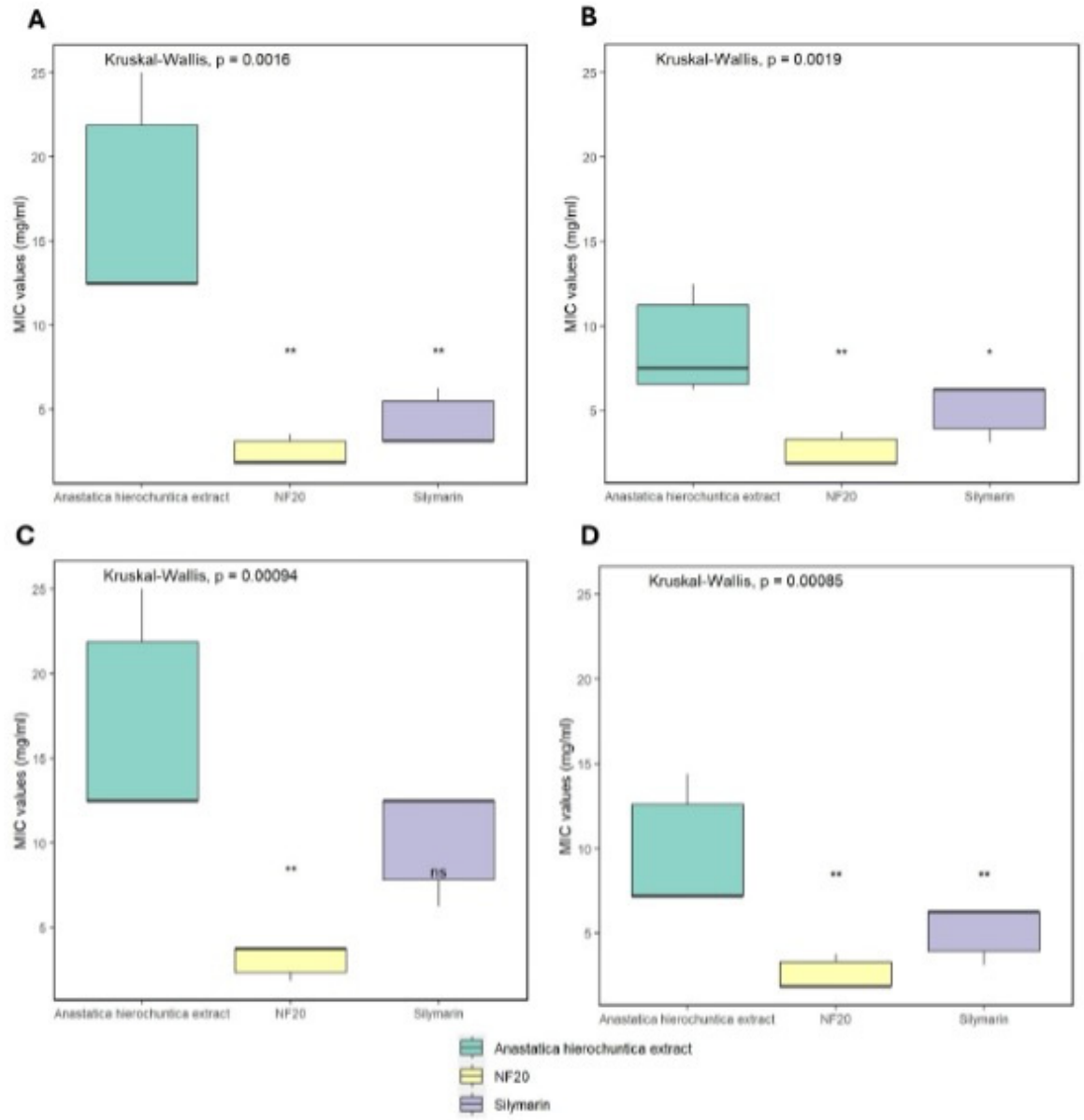

Figure 6. MIC values (mg/mL) of *A. hierochuntica* extract, NF20, and silymarin (n=9), against *Acinetobacter baumannii* ATCC 19606 (**A**), *Pseudomonas aeruginosa* PAO1 (**B**), *Staphylococcus aureus* ATCC 25923 (**C**), and *Aspergillus niger* ATCC32656 (**D**). MIC of NF20 was significantly lower than that of the *A. hierochuntica* extract against all tested strains. The MIC of silymarin was significantly lower than that of the extract in all strains except *Staphylococcus aureus* ATCC 25923.

3.3.2. Determination of Minimum Bactericidal Concentration (MBC) and Minimum Fungicidal Concentration (MFC)

Minimum Bactericidal concentration, for all tested preparations, was determined by the broth microdilution technique. All tested preparations showed bactericidal effect after 24 h of incubation at 37 °C. For *Acinetobacter baumannii,* MBC of NF20 (7.48 mg/mL) was significantly lower than both *A. hierochuntica* extract (33.5 mg/mL) and Silymarin (20.8 mg/mL) (Figure 7A). For *Pseudomonas aeruginosa*, MBC of NF20 (2.81 mg/mL) was significantly lower than both *A. hierochuntica* extract (16.6 mg/mL) and Silymarin (10.4 mg/mL) (Figure 7B). For *Staphylococcus aureus*, MBC of NF20 (5 mg/mL) was significantly lower than both *A. hierochuntica* extract (33.3 mg/mL) and Silymarin (20.8 mg/mL) (Figure 7C). However, there was no significant difference between MBC values of *A. hierochuntica* extract and Silymarin against all tested bacterial strains.

 doi:10.20944/preprints202410.1181.v1

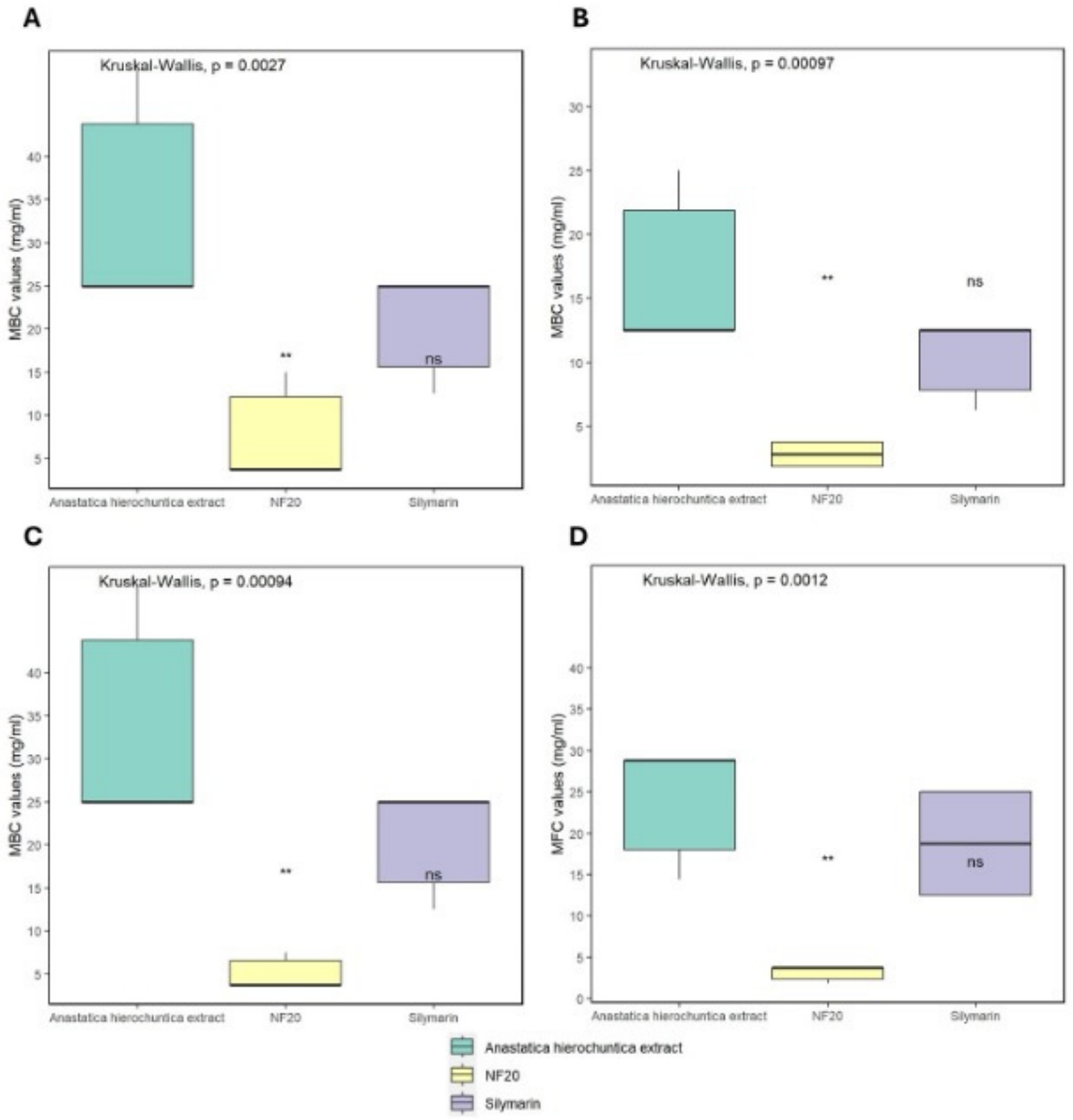

Figure 7. MBC/MFC values (mg/mL) of *A. hierochuntica* extract, NF20 and silymarin (n=9), against *Acinetobacter baumannii* ATCC 19606 (**A**), *Pseudomonas aeruginosa* PAO1 (**B**), *Staphylococcus aureus* ATCC 25923 (**C**), and *Aspergillus niger* ATCC32656 (**D**). MBC/MFC values of NF20 were significantly lower than both the *A. hierochuntica* extract and silymarin against all tested strains. There was no significant difference between MBC/MFC of silymarin and that of the *A. hierochuntica* extract against all tested strains.

Minimum fungicidal concentration (MFC) against *Aspergillus niger* was also determined by the broth microdilution technique. All tested preparations showed fungicidal effect after 24 h of incubation at 28 ± 2 °C. NF20 exhibited higher fungicidal activity (MFC=3.125 mg/mL) when compared to *A. hierochuntica* extract (MFC=24 mg/mL) and Silymarin (MFC=18.75 mg/mL) (Figure 7C).

3.3.3. Investigating the Biofilm Inhibitory Effect via Crystal Violet Technique

The biofilm inhibitory effect of NF20 was compared to that of *A. hierochuntica* extract against three bacterial standard strain by the crystal violet method. The biofilm inhibition activity of both preparations was determined at sub-MIC concentrations; 1/16, 1/8, ¼, and ½ X, where X is the calculated MIC; from 3.125 to 0.117 mg/mL for NF20, and from 8.3 to 0.546 mg/mL for the *A. hierochuntica* extract.

 doi:10.20944/preprints202410.1181.v1

NF20 showed significantly higher biofilm inhibition activity than that *A. hierochuntica* extract against all tested bacterial standard strains at all tested concentration (Student's t-test, *p* value <0.005, Figure 8) except at $^{1}/_{16}$X concentration for *Staphylococcus aureus* (t-test, *p* value =, 0.063, Figure 8C). Moreover, NF20 showed significantly higher biofilm inhibition activity when compared to Silymarin standard at sub-MIC concentrations; from 3.125 to 0.117 mg/mL for NF20 and from 12.5 to 0.2603 mg/mL for Silymarin against all tested bacterial standard strains at all tested concentration (Student's t-test, *p* value <0.05, Figure 9). These findings suggest that the nanofiber preparation significantly increased the biofilm inhibition activity of *A. hierochuntica* extract. These findings suggest that the nanofiber preparation significantly increased the biofilm inhibition activity of *Anastatica hierochuntica* extract.

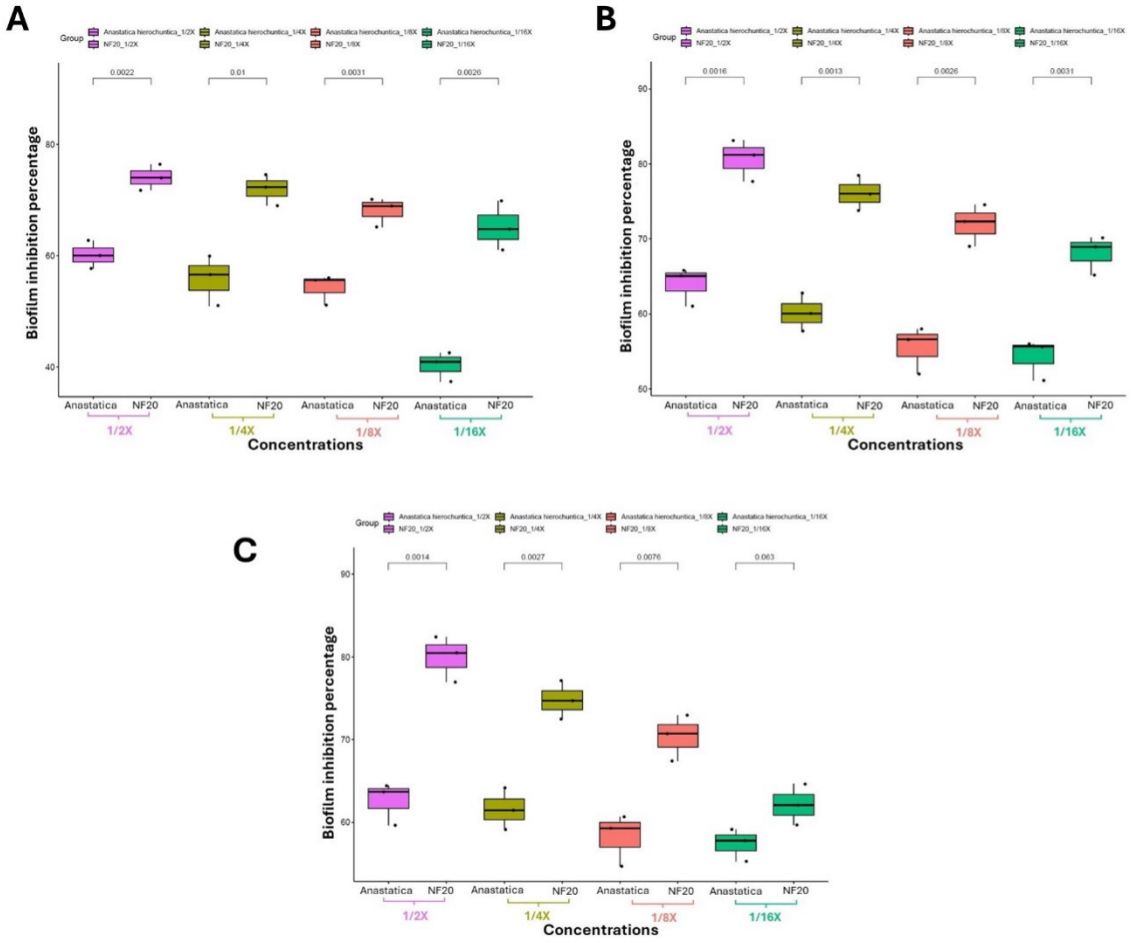

Figure 8. Biofilm inhibition activity of different concentrations ($^{1}/_{16}$, $^{1}/_{8}$, ¼, and ½ X, where X is the calculated MIC) of both *A. hierochuntica* extract and NF20 against *Acinetobacter baumannii* ATCC 19606 (**A**), *Pseudomonas aeruginosa* PAO1 (**B**) and *Staphylococcus aureus* ATCC 25923 (**C**).

 doi:10.20944/preprints202410.1181.v1

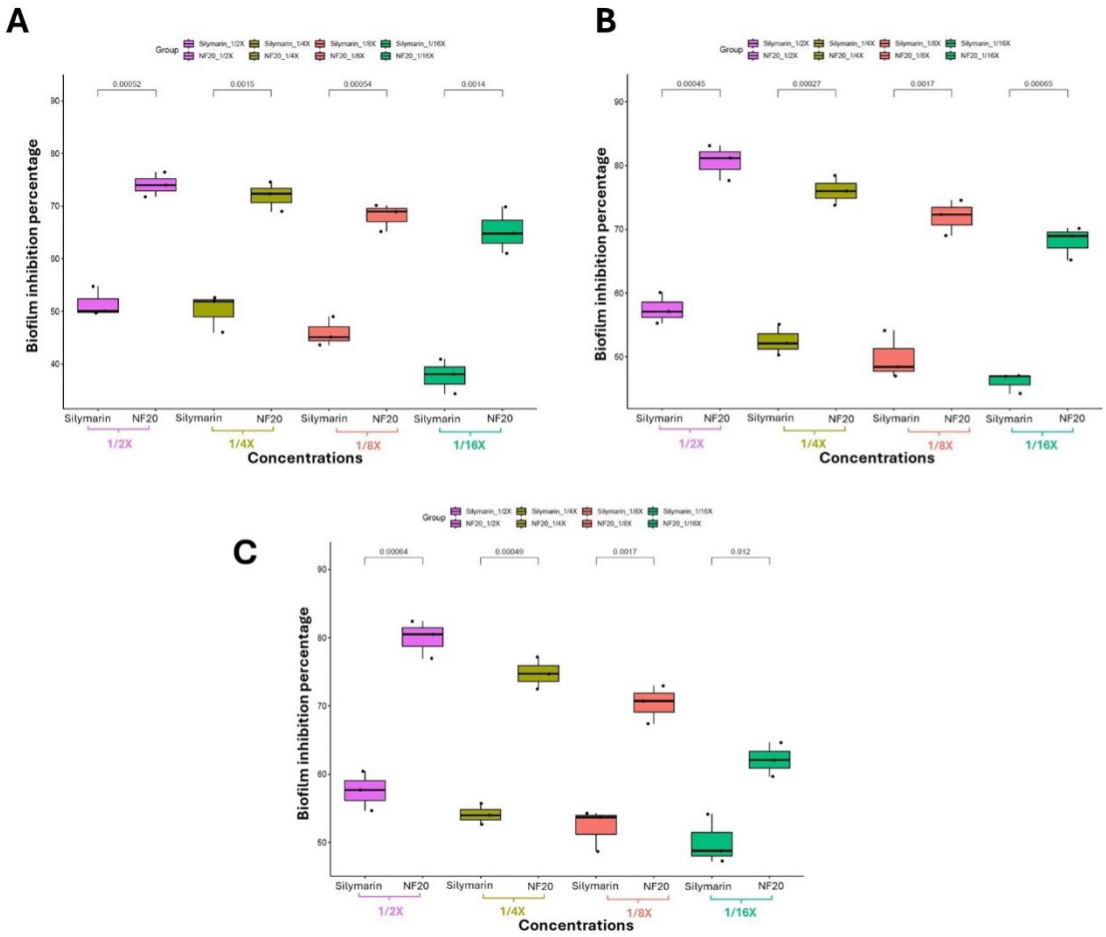

Figure 9. Biofilm inhibition activity of different concentrations ($^1/_{16}$, $^1/_8$, ¼, and ½ X, where X is the calculated MIC) of both NF20 and silymarin standard against *Acinetobacter baumannii* ATCC 19606 (**A**), *Pseudomonas aeruginosa* PAO1 (**B**) and *Staphylococcus aureus* ATCC 25923 (**C**).

3.4. Cell-line Studies; Wound Healing Assay

Wound healing process can be divided into four phases, as mentioned earlier. Ideally, the faster the rate of cellular migration to the wound site, the faster wound closure and healing takes place. Both events minimize the risk of permanent scarring. Fibroblasts contribute significantly to wound healing as they mainly support cellular growth and differentiation as well as speeding up the whole process through initiating the breakdown of blood clots and the formation of new ECM[52]. Wound healing assay (Scratch assay) was performed to assess the effectiveness of the selected extract-loaded NFs (NF20) in wound healing using HSF cell line. The results of %WC, as seen in Figure 10, demonstrate the significant benefits of extract loading within NFs (NF20) in accelerating wound healing and closure. After 72 h, %WC for NF20 was significantly larger ($P < 0.05$) than that of NFP (82.98±0.6% vs 36.94±1.1%, respectively). Microscopically speaking, the pictures of wound closure in Figure 11 highlight the enhanced rate of wound closure in the treatment group (NF20) as compared to NFP and the control groups. Such differences in the rate of wound closure and cell migration demonstrate the beneficial role that *Anastatica hierochuntica* extract plays in wound healing due to the synergistic activity of several constituents present in the extract such as silymarin isomers, which demonstrated significant epithelial regeneration and reduced inflammatory response upon its topical application on skin-wounded rats[53], and flavonoids which are capable of modulating inflammatory pathway together with stimulation of cellular proliferation and migration which lead to promoted tissue regeneration at the wound site[54], as well as the suitability of NFs as wound dressing to directly deliver the extract to the wound site.

 doi:10.20944/preprints202410.1181.v1

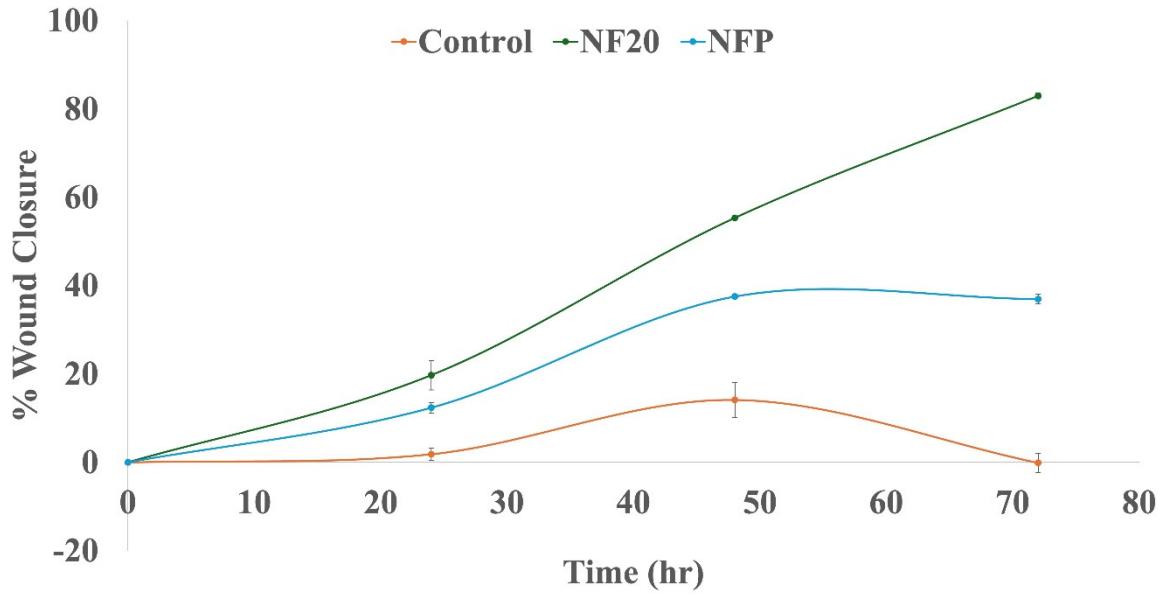

Figure 10. Representation of % WC against time (hr) indicates the superior benefits of the extract loaded NFs (NF20) in accelerating wound closure as compared to the plain NFs (NFP) and control groups.

 doi:10.20944/preprints202410.1181.v1

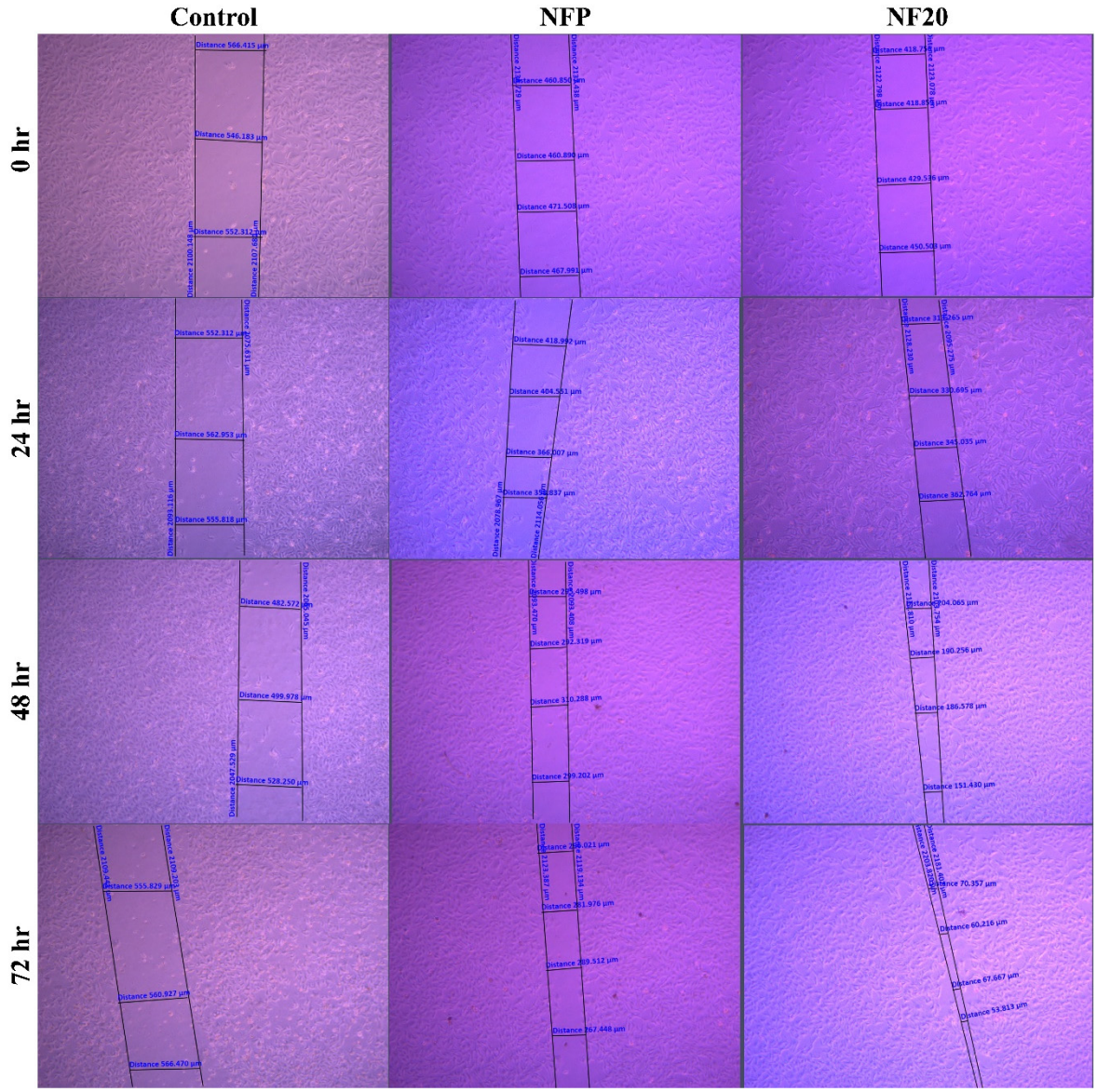

Figure 11. Images representing wound healing over 72 hr testing period confirming the superior benefits of the extract loaded NFs (NF20) in accelerating wound closure as compared to the plain NFs (NFP) and control groups.

4. Conclusion

This research focused on the antimicrobial properties of the unique plant *Anastatica hierochuntica* upon integration into nanofibers as wound dressing. The plant extract loaded nanofibers (NFs) were prepared via electrospinning, producing rod-like fibers with ridges around 240 nm in diameter. The loaded NFs exhibited hydrophilic characteristics and adequate mechanical properties that confirm their suitability for wound dressing.

The selected extract-loaded NFs (NF20) showed a controlled drug release. Tests against pathogens such as *Acinetobacter baumannii*, *Pseudomonas aeruginosa*, *Staphylococcus aureus*, and *Aspergillus niger* revealed the enhanced NFs antimicrobial activity as evidenced by reduced minimum inhibitory, bactericidal, and fungicidal concentrations compared to Silymarin standard. Further, the wound healing assay confirmed that the extract-loaded NFs accelerated healing. Future work should be focused on areas such as degradability testing of the fabricated NFs as well as macroscopical and histopathological assessment of the newly formed tissue. Overall, the findings of this research paper suggest the undeniable benefits of *A. hierochuntica* NFs in wound dressings.

Author contributions: Eman Abdelhakeem: Conceptualization, Methodology, Software, Formal analysis, Investigation, Resources, Review & Editing. **Mona M. Hashem:** Conceptualization, Methodology of phytochemical section, **Heba Attia:** Conceptualization, Methodology & Results analysis of microbiological section, **Mohamed A. Abdel Khalek:** Conceptualization, Methodology, Software, Formal analysis, Investigation, Resources, **Shaimaa M. Badr-Eldin** : Formal analysis, Review & Editing. **Islam M. Adel**: Conceptualization, Methodology, Software, Writing—Original Draft, Writing—Review & Editing.

Funding: This research work was funded by the Institutional Fund Projects under grant no. (IFPIP: 1695-249-1443). The authors gratefully acknowledge technical and financial support provided by the Ministry of Education and King Abdulaziz University, DSR, Jeddah, Saudi Arabia.

Acknowledgement: The authors would like to acknowledge the profound effort put in by Dr. Jihan Seid Hussein (Prof. of Medical Biochemistry, Medical Biochemistry Department, National Research Center) to accomplish the wound healing assays of the research.

Conflict of Interest: The authors of this work confirm that there is no conflict of interest.

References

1. Gilaberte, Y.; Prieto-Torres, L.; Pastushenko, I.; Juarranz, Á. Chapter 1 - Anatomy and Function of the Skin. In *Nanoscience in Dermatology*; Hamblin, M.R., Avci, P., Prow, T.W., Eds.; Academic Press: Boston, 2016; pp. 1–14 ISBN 978-0-12-802926-8.
2. Liang, Y.; Liang, Y.; Zhang, H.; Guo, B. Antibacterial Biomaterials for Skin Wound Dressing. *Asian J Pharm Sci* 2022, *17*, 353–384, doi:https://doi.org/10.1016/j.ajps.2022.01.001.
3. Zhang, X.; Wang, Y.; Gao, Z.; Mao, X.; Cheng, J.; Huang, L.; Tang, J. Advances in Wound Dressing Based on Electrospinning Nanofibers. *J Appl Polym Sci* 2024, *141*, e54746, doi:https://doi.org/10.1002/app.54746.
4. Tottoli, E.M.; Dorati, R.; Genta, I.; Chiesa, E.; Pisani, S.; Conti, B. Skin Wound Healing Process and New Emerging Technologies for Skin Wound Care and Regeneration. *Pharmaceutics* 2020, *12*, doi:10.3390/pharmaceutics12080735.
5. Velnar, T.; Bailey, T.; Smrkolj, V. The Wound Healing Process: An Overview of the Cellular and Molecular Mechanisms. *Journal of International Medical Research* 2009, *37*, 1528–1542, doi:10.1177/147323000903700531.
6. Guo, S.; DiPietro, L.A. Factors Affecting Wound Healing. *J Dent Res* 2010, *89*, 219–229, doi:10.1177/0022034509359125.
7. Enoch, S.; Leaper, D.J. Basic Science of Wound Healing. *Surgery (Oxford)* 2008, *26*, 31–37, doi:https://doi.org/10.1016/j.mpsur.2007.11.005.
8. Tottoli, E.M.; Dorati, R.; Genta, I.; Chiesa, E.; Pisani, S.; Conti, B. Skin Wound Healing Process and New Emerging Technologies for Skin Wound Care and Regeneration. *Pharmaceutics* 2020, *12*, doi:10.3390/pharmaceutics12080735.
9. Holloway, S.; Harding, K.G. Wound Dressings. *Surgery - Oxford International Edition* 2022, *40*, 25–32, doi:10.1016/j.mpsur.2021.11.002.
10. Kamoun, E.A.; Kenawy, E.-R.S.; Chen, X. A Review on Polymeric Hydrogel Membranes for Wound Dressing Applications: PVA-Based Hydrogel Dressings. *J Adv Res* 2017, *8*, 217–233, doi:https://doi.org/10.1016/j.jare.2017.01.005.
11. Kenry; Lim, C.T. Nanofiber Technology: Current Status and Emerging Developments. *Prog Polym Sci* 2017, *70*, 1–17, doi:https://doi.org/10.1016/j.progpolymsci.2017.03.002.
12. Yan, X.; Xiao, X.; Au, C.; Mathur, S.; Huang, L.; Wang, Y.; Zhang, Z.; Zhu, Z.; Kipper, M.J.; Tang, J.; et al. Electrospinning Nanofibers and Nanomembranes for Oil/Water Separation. *J. Mater. Chem. A* 2021, *9*, 21659–21684, doi:10.1039/D1TA05873H.
13. Sun, Y.; Cheng, S.; Lu, W.; Wang, Y.; Zhang, P.; Yao, Q. Electrospun Fibers and Their Application in Drug Controlled Release, Biological Dressings, Tissue Repair, and Enzyme Immobilization. *RSC Adv.* 2019, *9*, 25712–25729, doi:10.1039/C9RA05012D.
14. Memic, A.; Abdullah, T.; Mohammed, H.S.; Joshi Navare, K.; Colombani, T.; Bencherif, S.A. Latest Progress in Electrospun Nanofibers for Wound Healing Applications. *ACS Appl Bio Mater* 2019, *2*, 952–969, doi:10.1021/acsabm.8b00637.
15. Samadian, H.; Zamiri, S.; Ehterami, A.; Farzamfar, S.; Vaez, A.; Khastar, H.; Alam, M.; Ai, A.; Derakhshankhah, H.; Allahyari, Z.; et al. Electrospun Cellulose Acetate/Gelatin Nanofibrous Wound Dressing Containing Berberine for Diabetic Foot Ulcer Healing: In Vitro and in Vivo Studies. *Sci Rep* 2020, *10*, 8312, doi:10.1038/s41598-020-65268-7.
16. Wu, H.; Xie, H.; Tian, X.; Sun, Y.; Shi, B.; Zhou, Y.; Sheng, D.; Liu, X.; Yang, Y. Hard, Tough and Fast Self-Healing Thermoplastic Polyurethane. *Prog Org Coat* 2021, *159*, 106409, doi:https://doi.org/10.1016/j.porgcoat.2021.106409.

17. Liang, W.; Ni, N.; Huang, Y.; Lin, C. An Advanced Review: Polyurethane-Related Dressings for Skin Wound Repair. *Polymers (Basel)* 2023, *15*, doi:10.3390/polym15214301.
18. Yusof, J.; Mahdy, Z.A.; Noor, R.M. Use of Complementary and Alternative Medicine in Pregnancy and Its Impact on Obstetric Outcome. *Complement Ther Clin Pract* 2016, *25*, 155–163, doi:https://doi.org/10.1016/j.ctcp.2016.09.005.
19. Zin, S.R.M.; Kassim, N.M.; Alshawsh, M.A.; Hashim, N.E.; Mohamed, Z. Biological Activities of Anastatica Hierochuntica L.: A Systematic Review. *Biomedicine & Pharmacotherapy* 2017, *91*, 611–620, doi:https://doi.org/10.1016/j.biopha.2017.05.011.
20. Sobhy, E.; Tailang, M.; Benyounes, S.; Karunakaran, G. Antimalarial and Hepatoprotective Effects of Entire Plants of Anastatic Hierochuntica. 2011, *1*, 24–27.
21. abou elella, F.; Ahmed, E.; Gavamukulya, Y. Determination of Antioxidant and Anti-Inflammatory Activities, as Well as in Vitro Cytotoxic Activities of Extracts of Anastatica Hierochuntica (Kaff Maryam) against HeLa Cell Lines. *J Med Plant Res* 2016, *10*, 77–87, doi:10.5897/JMPR2015.6030.
22. AL-Saeed, A.; Jaber, N. Chemical Content and Antibacterial Activity of Some Extracts of Anastatica Hierochuntica Leaves. 2013, *4*.
23. Alatshan, A.; Qnais, E.; Wedyan, M.; Bseiso, Y.; Alzyoud, E.; Banat, R.; Alkhateeb, H. Antinociceptive and Antiinflammatory Activities of Anastatica Hierochuntica and Possible Mechanism of Action. *Indian J Pharm Sci* 2018, *80*, doi:10.4172/pharmaceutical-sciences.1000403.
24. Daur, I. Chemical Properties of the Medicinal Herb Kaff Maryam (Anastatica Hierochuntica L.) and Its Relation to Folk Medicine Use. *Afr J Microbiol Res* 2012, *6*, 5048–5051, doi:10.5897/AJMR12.755.
25. Alqudah, A.; AbuDalo, R.; Qnais, E.; Wedyan, M.; Qudah, T.; Oqal, M. Potential Anti-Inflammatory Activity of the Anastatica Hierochuntica Essential Oil. *Journal of Essential Oil Research* 2023, *35*, 1–10, doi:10.1080/10412905.2022.2118878.
26. Zin, S.R.M.; Kassim, N.M.; Alshawsh, M.A.; Hashim, N.E.; Mohamed, Z. Biological Activities of Anastatica Hierochuntica L.: A Systematic Review. *Biomedicine & Pharmacotherapy* 2017, *91*, 611–620, doi:https://doi.org/10.1016/j.biopha.2017.05.011.
27. Amin Mohamed, A.; Khalil, A.; El-Beltagi, H. Antioxidant and Antimicrobial Properties of Kaff Maryam(Anastatica Hierochuntica) and Doum Palm (Hyphaene Thebaica). *Grasas y Aceites* 2010, *61*, 67–75, doi:10.3989/gya.064509.
28. Petrásková, L.; Káňová, K.; Biedermann, D.; Křen, V.; Valentová, K. Simple and Rapid HPLC Separation and Quantification of Flavonoid, Flavonolignans, and 2,3-Dehydroflavonolignans in Silymarin. *Foods* 2020, *9*, doi:10.3390/foods9020116.
29. Adel, I.M.; ElMeligy, M.F.; Elkasabgy, N.A. Conventional and Recent Trends of Scaffolds Fabrication: A Superior Mode for Tissue Engineering. *Pharmaceutics* 2022, *14*, doi:10.3390/pharmaceutics14020306.
30. Salam, A.; Khan, M.Q.; Hassan, T.; Hassan, N.; Nazir, A.; Hussain, T.; Azeem, M.; Kim, I.S. In-Vitro Assessment of Appropriate Hydrophilic Scaffolds by Co-Electrospinning of Poly(1,4 Cyclohexane Isosorbide Terephthalate)/Polyvinyl Alcohol. *Sci Rep* 2020, *10*, 19751, doi:10.1038/s41598-020-76471-x.
31. Eldeeb, A.E.; Salah, S.; Amer, M.S.; Elkasabgy, N.A. 3D Nanocomposite Alginate Hydrogel Loaded with Pitavastatin Nanovesicles as a Functional Wound Dressing with Controlled Drug Release; Preparation, in-Vitro and in-Vivo Evaluation. *J Drug Deliv Sci Technol* 2022, *71*, 103292, doi:https://doi.org/10.1016/j.jddst.2022.103292.
32. Samy, M.; Ekram, B.; Abd El-Hady, B.M.; Ayoub, M.M.H. In Vitro Release Study of Electrospun Poly(ε-Caprolactone)/Gelatin Nanofiber Mats Loaded with 5-Fluorouracil. *Polymer Bulletin* 2024, *81*, 3953–3972, doi:10.1007/s00289-023-04930-2.
33. Adel, I.M.; ElMeligy, M.F.; Abdelkhalek, A.A.; Elkasabgy, N.A. Design and Characterization of Highly Porous Curcumin Loaded Freeze-Dried Wafers for Wound Healing. *European Journal of Pharmaceutical Sciences* 2021, *164*, 105888, doi:https://doi.org/10.1016/j.ejps.2021.105888.
34. Elshikh, M.; Ahmed, S.; Funston, S.; Dunlop, P.; McGaw, M.; Marchant, R.; Banat, I.M. Resazurin-Based 96-Well Plate Microdilution Method for the Determination of Minimum Inhibitory Concentration of Biosurfactants. *Biotechnol Lett* 2016, *38*, 1015–1019, doi:10.1007/s10529-016-2079-2.
35. Haney, E.; Trimble, M.; Hancock, R. Microtiter Plate Assays to Assess Antibiofilm Activity against Bacteria. *Nat Protoc* 2021, *16*, 1–18, doi:10.1038/s41596-021-00515-3.
36. O'Toole, G.A. Microtiter Dish Biofilm Formation Assay. *JoVE* 2011, e2437, doi:doi:10.3791/2437.
37. Racine, J. RStudio: A Platform-Independent IDE for R and Sweave. *Journal of Applied Econometrics* 2012, *27*, doi:10.2307/41337225.
38. Kauanova, S.; Urazbayev, A.; Vorobjev, I. The Frequent Sampling of Wound Scratch Assay Reveals the "Opportunity" Window for Quantitative Evaluation of Cell Motility-Impeding Drugs. *Front Cell Dev Biol* 2021, *9*, doi:10.3389/fcell.2021.640972.
39. Hussein, J.; ELBana, M.; Abdel Latif, Y.; Saleh, S.; Tolba, E. Wound Healing Activity of Cotton Fabrics Loaded with Silver Nanoparticles in Experimental Model of Diabetes. *Biomedical and Pharmacology Journal* 2023, *16*, 53–65, doi:10.13005/bpj/2587.

40. Meenatchi, V.; Bhaskar, R.; Sood, A.; Han, S.S. Preparation of β-Cyclodextrin Derivatives/Metamizole Inclusion Complex Nanofibers: Characterization, Drug Release, and Wound Scratch Assay. *J Drug Deliv Sci Technol* 2024, *97*, 105752, doi:https://doi.org/10.1016/j.jddst.2024.105752.
41. Morilla-Herrera, J.C.; Morales-Asencio, J.M.; Gómez-González, A.J.; Díez-De Los Ríos, A.; Lupiáñez-Pérez, I.; Acosta-Andrade, C.; Aranda-Gallardo, M.; Moya-Suárez, A.B.; Kaknani-Uttumchandani, S.; García-Mayor, S. Effectiveness of a Hydrophobic Dressing for Microorganisms' Colonization of Vascular Ulcers: Protocol for a Randomized Controlled Trial (CUCO-UV Study). *J Adv Nurs* 2020, *76*, 2191–2197, doi:https://doi.org/10.1111/jan.14412.
42. Hamdan, N.; Yamin, A.; Hamid, S.A.; Khodir, W.K.W.A.; Guarino, V. Functionalized Antimicrobial Nanofibers: Design Criteria and Recent Advances. *J Funct Biomater* 2021, *12*, doi:10.3390/jfb12040059.
43. Yang, S.; Lan, L.; Gong, M.; Yang, K.; Li, X. An Asymmetric Wettable PCL/Chitosan Composite Scaffold Loaded with IGF-2 for Wound Dressing. *J Biomater Appl* 2022, *37*, 577–587, doi:10.1177/08853282221110315.
44. Liu, L.; Sun, H.; Zhang, J.; Xu, B.; Gao, Y.; Qi, D.; Mao, Z.; Wu, J. Trilayered Fibrous Dressing with Wettability Gradient for Spontaneous and Directional Transport of Massive Exudate and Wound Healing Promotion. *Advanced Fiber Materials* 2023, *5*, 574–587, doi:10.1007/s42765-022-00239-3.
45. Daur, I. Chemical Properties of the Medicinal Herb Kaff Maryam (Anastatica Hierochuntica L.) and Its Relation to Folk Medicine Use. *Afr J Microbiol Res* 2012, *6*, 5048–5051, doi:10.5897/AJMR12.755.
46. Kalra, A.; Lowe, A. Mechanical Behaviour of Skin: A Review. *Journal of Material Science & Engineering* 2016, *5*, doi:10.4172/2169-0022.1000254.
47. Taha, E.; Nour, S.A.; Mamdouh, W.; Naguib, M.J. Investigating the Potential of Highly Porous Zopiclone-Loaded 3D Electrospun Nanofibers for Brain Targeting via the Intranasal Route. *Int J Pharm* 2024, *660*, 124230, doi:https://doi.org/10.1016/j.ijpharm.2024.124230.
48. Hou, C.; Newton, M.A.A.; Xin, B.; Li, T. Preparation and Characterization of Unidirectional Water-Transported Bilayer PLA/ZnO-PAN/SPA Nanofibrous Membrane for Wound Healing. *Colloids Surf A Physicochem Eng Asp* 2023, *676*, 132308, doi:https://doi.org/10.1016/j.colsurfa.2023.132308.
49. Suryamathi, M.; Ruba, C.; Viswanathamurthi, P.; Balasubramanian, V.; Perumal, P. Tridax Procumbens Extract Loaded Electrospun PCL Nanofibers: A Novel Wound Dressing Material. *Macromol Res* 2019, *27*, 55–60, doi:10.1007/s13233-019-7022-7.
50. Lee, Y.-H.; Kang, B.-K.; Kim, H.-D.; Yoo, H.-J.; Kim, J.-S.; Huh, J.-H.; Jung, Y.-J.; Lee, D.-J. Effect of Hot Pressing/Melt Mixing on the Properties of Thermoplastic Polyurethane. *Macromol Res* 2009, *17*, 616–622, doi:10.1007/BF03218918.
51. Asefnejad, A.; Khorasani, M.T.; Behnamghader, A.; Farsad, B.; Bonakdar, S. Manufacturing of Biodegradable Polyurethane Scaffolds Based on Polycaprolactone Using a Phase Separation Method: Physical Properties and in Vitro Assay. *Int J Nanomedicine* 2011, *6*, 2375–2384, doi:10.2147/IJN.S15586.
52. P., B. Wound Healing and the Role of Fibroblasts. *J Wound Care* 2013, *22*, 407–412, doi:10.12968/jowc.2013.22.8.407.
53. Oryan, A.; Naeini, A.; Moshiri, A.; Mohammadalipour, A.; Tabandeh, M. reza Modulation of Cutaneous Wound Healing by Silymarin in Rats. *J Wound Care* 2012, *21*, 457–464, doi:10.12968/jowc.2012.21.9.457.
54. Zulkefli, N.; Che Zahari, C.N.M.; Sayuti, N.H.; Kamarudin, A.A.; Saad, N.; Hamezah, H.S.; Bunawan, H.; Baharum, S.N.; Mediani, A.; Ahmed, Q.U.; et al. Flavonoids as Potential Wound-Healing Molecules: Emphasis on Pathways Perspective. *Int J Mol Sci* 2023, *24*, doi:10.3390/ijms24054607.